Staggered Nonlinear Spin Generations in Centrosymmetric Altermagnets under Electric Current

Jie Zhang(张洁), Ruijing Fang(房瑞菁), Zhichao Zhou(周智超), and Xiao Li(李晓)*

Center for Quantum Transport and Thermal Energy Science, Institute of Physics Frontiers and Interdisciplinary Sciences, School of Physics and Technology, Nanjing Normal University, Nanjing 210023, China

(Received 2 December 2025; accepted manuscript online 6 January 2026)

Current-induced spin generations are of significant importance for electrically controllable magnetization. Due to symmetry constraints, linear spin generation is absent in centrosymmetric magnets and nonlinear contributions become crucial. However, nonlinear spin generations have few examples in centrosymmetric compensated magnets with opposite-spin sublattices, which hinders electric control of associated magnetization. Here, we study nonlinear spin generations in altermagnets, a new type of compensated magnets. In a square altermagnetic model, both staggered and uniform nonlinear spin generations appear at opposite-spin sublattices. They vary as the magnetization direction rotates, with emerging out-of-plane components that can be utilized in perpendicular magnetization switching of high-density storage devices. By first-principles calculations, out-of-plane, staggered nonlinear spin generations are found to be considerable in a typical altermagnet, Fe_2Se_2O monolayer. Our findings provide opportunities for electrically manipulating magnetization and designing energy-efficient magnetic devices based on compensated magnets.

DOI: 10.1088/0256-307X/43/2/020711 CSTR: 32039.14.0256-307X.43.2.020711

1. Introduction. Electric control of magnetization has recently received significant attention. In magnets, current-induced spin generations and associated torques play a role of effective magnetic field, which has enormous applications in spintronics, e.g., driving magnetization switching and domain-wall motion.[1–3] Specifically to antiferromagnets, it has been theoretically recognized that staggered spin generations on antiferromagnetically coupled sites are essential for manipulating magnetization dynamics,[4,5] and the reorientation of antiferromagnetic Néel vector has subsequently been realized under the action of electric current in experiments.[6–9] Previous studies have primarily focused on magnetic materials with inversion symmetry breaking, which is regarded as a necessary condition for linear spin generations under electric current.[4,5] As spin generation has recently been extended to nonlinear regime, electric control of magnetization is also expected in centrosymmetric magnets through nonlinear spin responses to electric field.[10,11] However, compared with ferromagnets, there have been few studies on nonlinear spin generations in compensated magnets with opposite-spin sublattices, and the site dependence of spin generations remains elusive.

On the other hand, altermagnetism, as a new type of compensated magnetic phase, exhibits exotic characteristics.[12–17] Altermagnets have opposite-spin sublattices that are connected by rotational or mirror symmetry in real space, while spin-split bands appear in momentum space. For the new magnetic phase, the primary method to control magnetization reorientation still relies on applying magnetic fields,[18,19] with few studies on electric control. Therefore, centrosymmetric altermagnets with opposite-spin sublattices provide a fertile platform for studying nonlinear spin generations and associated site dependence, which is expected to enable electric control of magnetization in compensated magnets.

In this work, we study nonlinear spin generations in centrosymmetric altermagnets, by combining symmetry analyses, tight-binding model, and first-principles calculations. In a two-dimensional square altermagnetic model with orbital ordering, both staggered and uniform spin generations are found on two opposite-spin sublattices. Their magnitudes and signs vary with the magnetization direction, with emerging out-of-plane staggered spin components. The staggered spin generations can be used to regulate magnetic dynamics of opposite-spin sublattices, and the out-of-plane spin generations are particularly desirable for high-density storage devices based on out-of-plane anisotropic magnets. Taking the Fe_2Se_2O monolayer as a typical example of two-dimensional altermagnets, first-principles calculations of nonlinear spin generations are then performed, and corresponding results support the findings from the model. Out-of-plane staggered nonlinear spin generations in the monolayer reach the order of $10^4\,\mu_B/V^2$, which is larger than that of previous studied ferromagnet.[10] Our studies extend nonlinear spin generations to compensated magnets, and pave the way for manipulating magnetization of opposite-spin sublattices by electric means.

2. Crystal Structure and Symmetry Analyses. We

*Corresponding author. Email: lixiao@njnu.edu.cn

© 2026 Chinese Physical Society and IOP Publishing Ltd. All rights, including for text and data mining, AI training, and similar technologies, are reserved.

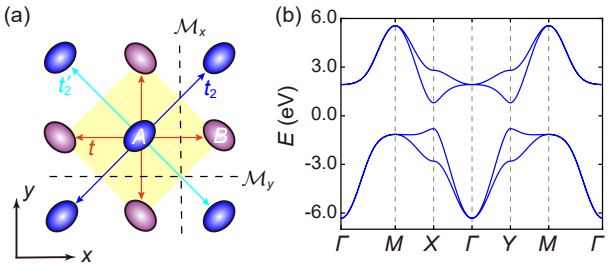

Fig. 1. Orbital ordering and band structure of an altermagnetic square lattice. (a) Local atomic orbitals in a square lattice. The blue and purple ellipses stand for two mutually perpendicular orbitals on A and B sublattices, which leads to anisotropic NNN hoppings denoted by t_2 and t_2'. The A and B sublattices are related by mirror symmetries, $\mathcal{M}_{x/y}$. The yellow shade represents a unit cell of the lattice. (b) Band structure of the lattice. The parameters $t = t_2 = J_{\rm ex} = -1.0\,{\rm eV}$, $t_2' = -0.1\,{\rm eV}$, and $t_{\rm soc} = 0.8\,{\rm eV}$.

first consider a two-dimensional altermagnetic model of a square lattice with anisotropic hopping parameters,[20–22] which is shown in Fig. 1(a). The square lattice includes two inequivalent sublattices, denoted as A and B, which have different orbital orderings. That is, two anisotropic orbitals at the A and B sublattices exhibit the same shape but with mutually perpendicular orientations. Moreover, considering magnetic ordering, there are opposite magnetic moments at the A and B sublattices. From the view of the crystal symmetry, the whole lattice, as well as the A and B sulattices, has the inversion symmetry $\mathcal{P}$. Owing to the presence of the orbital ordering, the A and B sublattices cannot be connected by the combined symmetry of $\mathcal{P}$ and time reversal $\mathcal{T}$, which leads to the altermagnetic order.[20] Besides, there are two mirror planes, $\mathcal{M}_x$ and $\mathcal{M}_y$, whose normal directions are along the x-axis and y-axis, respectively; they connect the two sublattices.

Based on the above symmetries, symmetry analyses of current-induced spin generations, $\delta\boldsymbol{s}$, in the square lattice are performed. Firstly, the presence of the $\mathcal{P}$ symmetry excludes the linear spin response to an applied electric field, i.e., $\delta\boldsymbol{s} \propto \boldsymbol{E}$, where $\boldsymbol{E}$ represents the applied electric field. It is because under the $\mathcal{P}$ operation, $\delta\boldsymbol{s}$ is invariant, whereas $\boldsymbol{E}$ is reversed, rendering the linear relationship invalid. Although the linear spin response is absent, the quadratic spin response is likely to become the leading contribution. The quadratic spin response to the applied electric field can be expressed as

$$\delta s_a = \chi_{abc} E_b E_c, \tag{1}$$

where χ_{abc} is the nonlinear response tensor, with the subscripts a, b, and c represents Cartesian coordinates. While a denotes the spin direction, b and c denote directions of electric fields. The Einstein summation convention is adopted in the equation. As for the quadratic spin response, the product of two electric-field components, as well as $\delta\boldsymbol{s}$, is invariant under the $\mathcal{P}$ operation; the response is thus symmetry-allowed in the centrosymmetric lattice. Further considering that the quadratic spin responses have two contributions—the $\mathcal{T}$-odd part arising from the Berry connection polarizability[10] and the $\mathcal{T}$-even part arising from the anomalous spin polarizability dipole[11]—χ_{abc} can be divided into $\chi^{\rm o}_{abc}$ and $\chi^{\rm e}_{abc}$. The related definitions and expressions for these two parts are provided in the Supplementary Materials (SM). Besides, when distinguishing the A and B sublattices, an extra subscript, $i = A$ or B, is added to the tensor χ and the spin generation $\delta\boldsymbol{s}$. The tensor element $\chi^{\rm o/e}_{abc,i}$ obeys the symmetry transformation rule,

$$\chi^{\rm o/e}_{a'b'c',i'} = \eta_{\mathcal{T}} \det(O) O_{a'a} O_{b'b} O_{c'c} \chi^{\rm o/e}_{abc,i}. \tag{2}$$

Here, O is a unitary matrix of a point group operation, which relates the sublattices i and i'. When $\chi^{\rm o}_{abc,i}$ is considered, the factor $\eta_{\mathcal{T}} = +1$ for a non-primed operation without $\mathcal{T}$, and $\eta_{\mathcal{T}} = -1$ for a primed operation that combines a spatial operation and $\mathcal{T}$. As for $\chi^{\rm e}_{abc,i}$, $\eta_{\mathcal{T}} = +1$ for both non-primed and primed operations.

According to Eq. (2), possible spin generations on A and B sublattices are analyzed for highly symmetric directions of local magnetic moments, as listed in Table 1. In the table, the symmetry operations connecting different sublattices, $\mathcal{M}_{x/y}$, are used to explore the relationship between δs_A and δs_B, while the symmetry operations $C_2^z\mathcal{T}$ or C_2^z transform the sublattices into themselves and determines the presence or absence of spin generations. Further considering the setup of two-dimensional transport experiment, applied electric fields are restricted to the xy plane and oriented along the same direction. When the local magnetic moments are aligned along the x-axis, staggered spin generations are found on the two sublattices, that is $\delta s_A = -\delta s_B$ for $\chi^{\rm o}_{xxx}$, $\chi^{\rm o}_{xyy}$, $\chi^{\rm e}_{zxx}$, and $\chi^{\rm e}_{zyy}$. Besides, spin generations on two sublattices are uniform, i.e., $\delta s_A = \delta s_B$, for $\chi^{\rm o}_{yxx}$ and $\chi^{\rm o}_{yyy}$. As for local magnetic moments along the y-axis, staggered and uniform spin generations are also found for different tensor elements of the nonlinear spin response. On the other hand, when the local magnetic moments are aligned along the z-axis, only staggered, out-of-plane spin generations occur on the two sublattices for electric fields applied along either the x- or y-axis.

Table 1. Symmetry constraints on tensor elements of nonlinear spin responses. The first and second lines list directions of local magnetic moments and corresponding magnetic point group symmetries, respectively. For each tensor element from the third to the eighth line, "+", "−" and "×" denote uniform, staggered and vanishing spin generations on two sublattices, respectively.

	$M \parallel x$	$M \parallel y$	$M \parallel z$
$\hat{O}$	$\mathcal{M}_y, C_2^z\mathcal{T}$	$\mathcal{M}_x, C_2^z\mathcal{T}$	$\mathcal{M}_x, \mathcal{M}_y, C_2^z$
$\chi^{\rm o/e}_{xxx}$	−/×	+/×	×/×
$\chi^{\rm o/e}_{yxx}$	+/×	−/×	×/×
$\chi^{\rm o/e}_{zxx}$	×/−	×/−	−/−
$\chi^{\rm o/e}_{xyy}$	−/×	+/×	×/×
$\chi^{\rm o/e}_{yyy}$	+/×	−/×	×/×
$\chi^{\rm o/e}_{zyy}$	×/−	×/−	−/−

According to the above symmetry analyses, there are two points worthy of attention. Firstly, staggered nonlinear spin generations are symmetry-allowed and highly desirable for effective switching of local magnetic moments in centrosymmetric compensated magnets. This is analogous to the role of the linear spin generation in noncentrosymmetric antiferromagnets.[23,24] Besides, uniform spin generations found here are likely to serve as a spin source for reorienting the magnetic moments of adjacent materials. Secondly, out-of-plane spin components can be generated, which is crucial for field-free perpendicular magnetization reversal in out-of-plane anisotropic magnets used high-density storage devices.[25–27]

3. Model Calculations of Nonlinear Spin Generations. Armed with the symmetry analyses, we then employ a tight-binding Hamiltonian of the altermagnetic square lattice to calculate electronic band structure and spin generations. Using $\{\psi_{A,\uparrow},\psi_{A,\downarrow},\psi_{B,\uparrow},\psi_{B,\downarrow}\}$ as a basis set, the Hamiltonian reads

$$\begin{aligned} H =\ & t\sum_{\langle i,j\rangle,\alpha} c^{\dagger}_{i,\alpha}c_{j,\alpha} + t_2\sum_{\langle\langle i,j\rangle\rangle,\alpha} c^{\dagger}_{i,\alpha}c_{j,\alpha} \\ & + t_2'\sum_{\langle\langle i,j\rangle\rangle,\alpha} c^{\dagger}_{i,\alpha}c_{j,\alpha} - J_{\rm ex}\sum_{i,\alpha,\beta}\boldsymbol{S}_i\cdot c^{\dagger}_{i,\alpha}\boldsymbol{\sigma}_{\alpha\beta}c_{i,\beta} \\ & + {\rm i}t_{\rm soc}\sum_{\langle i,j\rangle,\alpha,\beta}\nu_{ij}c^{\dagger}_{i,\alpha}\sigma^{z}_{\alpha\beta}c_{j,\beta}. \end{aligned} \tag{3}$$

In the basis set, $\psi_{i,\alpha}$ denotes the wave function of the sublattice i with spin α ($\alpha=\uparrow$ or $\downarrow$). The Hamiltonian includes five terms, corresponding respectively to nearest-neighbor (NN) hoppings, two kinds of anisotropic next-nearest-neighbor (NNN) hoppings, exchange interaction between itinerant spins and local magnetic moments, and intrinsic spin–orbit coupling (SOC) arising from NN hoppings. $c^{\dagger}_{i,\alpha}(c_{i,\alpha})$ is the creation (annihilation) operator of an electron. While t represents the NN hopping strength, t_2 and t_2' denote the strengths of the anisotropic NNN hoppings, as illustrated in Fig. 1(a). $J_{\rm ex}$ and $t_{\rm soc}$ quantify the strengths of the exchange interaction and SOC, respectively. $\boldsymbol{S}_i$ represents the unit vector of local magnetic moment, with $\boldsymbol{S}_A=-\boldsymbol{S}_B$ for the altermagnet with opposite-spin sublattices. $\boldsymbol{\sigma}=(\sigma_x,\sigma_y,\sigma_z)$ denotes the spin Pauli matrices. For the horizontal NN hoppings from sublattice A (B) to sublattice B (A) in Fig. 1(a), ν_{ij} in the SOC term takes the value -1 ($+1$). As for the vertical hoppings, ν_{ij} reverses its sign.

Figure 1(b) demonstrates the band structure of the altermagnetic square lattice with magnetization along the z-axis. It is seen that there are four bands, indicating the spin degeneracy is lifted for the altermagnetic order. Besides, for the parameters considered here, the valence band maximum and conduction band minimum are located at the high-symmetric X and Y points, forming two valleys for both bands. The two valleys are degenerate, a property protected by the mirror symmetries $\mathcal{M}_{x/y}$.[28] The tight-binding band structure is similar to the first-principle one of the Fe_2Se_2O monolayer,[29] which will be studied later.

According to the tight-binding Hamiltonian (3), we further calculate $\mathcal{T}$-odd and $\mathcal{T}$-even quadratic spin generations, as shown in Figs. 2 and 3, respectively, while linear spin generations are verified to be zero. In Figs. 2 and 3, the nonlinear spin generations, $\chi^{\rm o/e}_{abc,i}$, are presented as functions of the direction of local magnetic moment, with the electric field applied along the x-axis, i.e., $b=c=x$ in Eq. (1), and with a fixed chemical potential, $\mu=1.0\,{\rm eV}$. The direction of the local magnetic moment at sublattice A, $\boldsymbol{S}_A$, is described by two angles: the azimuthal angle ϕ and the canting angle θ, where $\theta=0$ denotes an in-plane magnetic moment. Given $\boldsymbol{S}_A=-\boldsymbol{S}_B$ for the altermagnet, ϕ and θ also parameterize the direction of the Néel vector. Figures 2(a) and 2(b) demonstrate the evolutions of the $\mathcal{T}$-odd part with varying ϕ in the equatorial plane ($\theta=0$) and with varying θ in the meridional plane passing through the x-axis ($\phi=0$), respectively.

In Fig. 2(a), it is seen that the in-plane spin generations, $\chi^{\rm o}_{xxx,A}$, $\chi^{\rm o}_{xxx,B}$, $\chi^{\rm o}_{yxx,A}$, and $\chi^{\rm o}_{yxx,B}$, exhibit trigonometric dependence on ϕ with nonzero initial phases, whereas the out-of-plane spin generations, $\chi^{\rm o}_{zxx,A}$ and $\chi^{\rm o}_{zxx,B}$, vanish. When $\phi=0$, π or 2π, $\chi^{\rm o}_{xxx,A}=-\chi^{\rm o}_{xxx,B}$, corresponding to staggered spin generations; and $\chi^{\rm o}_{yxx,A}=\chi^{\rm o}_{yxx,B}$, corresponding to uniform spin generations. When $\phi=\pi/2$ or $3\pi/2$, $\chi^{\rm o}_{xxx}$ and $\chi^{\rm o}_{yxx}$ become uniform and staggered, respectively. The results agree with the symmetry analyses in Table 1. Besides, when ϕ takes other values, the in-plane spin generations on the A and B sublattices are neither equal nor opposite, indicating coexistence of both staggered and uniform contributions. We thus decompose the spin generations into a staggered contribution λ_{abc} and a uniform contribution ξ_{abc}: $\chi^{\rm o}_{abc,A}=\lambda_{abc}+\xi_{abc}$, $\chi^{\rm o}_{abc,B}=\xi_{abc}-\lambda_{abc}$. Figures 2(c) and 2(d) present λ_{abc} and ξ_{abc} as functions of ϕ for $\chi^{\rm o}_{xxx}$ and $\chi^{\rm o}_{yxx}$, respectively. For $\chi^{\rm o}_{xxx}$ ($\chi^{\rm o}_{yxx}$), the staggered and uniform contributions look like cosine (sine) and sine (cosine) functions of ϕ, respectively, without phase shift. The amplitude of the staggered contribution is approximately twice that of the uniform one. Therefore, both the staggered and uniform spin generations act on two sublattices of the altermagnet and jointly determine its magnetization dynamics.

In Fig. 2(b), with the canting angle θ varied in the meridional plane passing through the x-axis, the $\mathcal{T}$-odd nonlinear spin generations, $\chi^{\rm o}_{xxx}$, $\chi^{\rm o}_{yxx}$, and $\chi^{\rm o}_{zxx}$, are all nonvanishing. $\chi^{\rm o}_{xxx}$ and $\chi^{\rm o}_{zxx}$ are always staggered on the A and B sublattices, while $\chi^{\rm o}_{yxx}$ is uniform—a consequence ensured by the mirror symmetry $\mathcal{M}_y$ and derivable from Eq. (2).

On the other hand, figures 3(a) and 3(b) show the $\mathcal{T}$-even nonlinear spin generations as functions of ϕ and θ, respectively. Components of the $\mathcal{T}$-even parts are staggered or uniform on the A and B sublattices, similar to those of the $\mathcal{T}$-odd parts.

When focusing on out-of-plane spin generations, not only the $\mathcal{T}$-odd part $\chi^{\rm o}_{zxx}$ but also $\mathcal{T}$-even part $\chi^{\rm e}_{zxx}$ are staggered, and the out-of-plane components are comparable in magnitude to the in-plane ones. These staggered out-of-plane components are likely to be utilized for perpendicular magnetization switching in high-density storage devices based on out-of-plane anisotropic magnets with

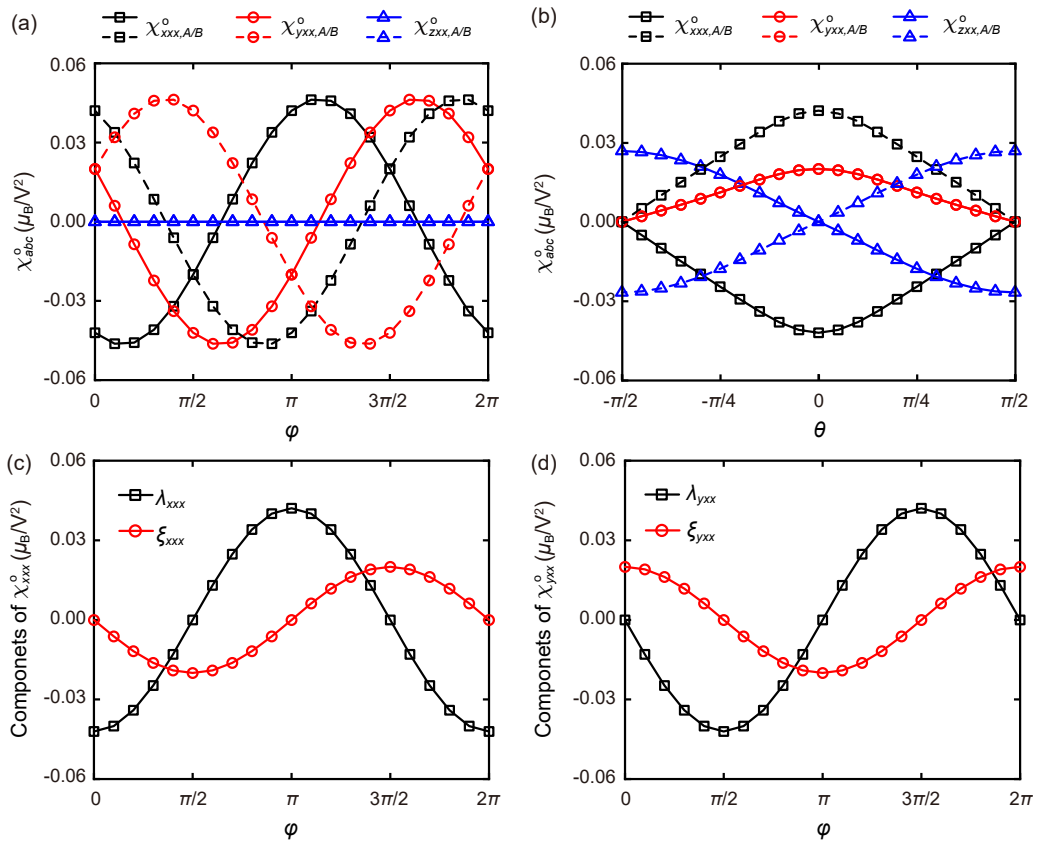

Fig. 2. $\mathcal{T}$-odd nonlinear spin generations in an altermagnetic square lattice. (a) Evolutions of $\chi^{\rm o}_{xxx,i}$, $\chi^{\rm o}_{yxx,i}$, and $\chi^{\rm o}_{zxx,i}$ as functions of the azimuthal angle ϕ with a fixed canting angle $\theta = 0$. (b) Evolutions of $\chi^{\rm o}_{xxx,i}$, $\chi^{\rm o}_{yxx,i}$, and $\chi^{\rm o}_{zxx,i}$ as functions of θ with fixed $\phi = 0$. (c) and (d) The staggered contribution λ_{abc} and the uniform contribution ξ_{abc} as functions of ϕ for $\chi^{\rm o}_{xxx}$ and $\chi^{\rm o}_{yxx}$, respectively. The chemical potential is set to 1 eV.

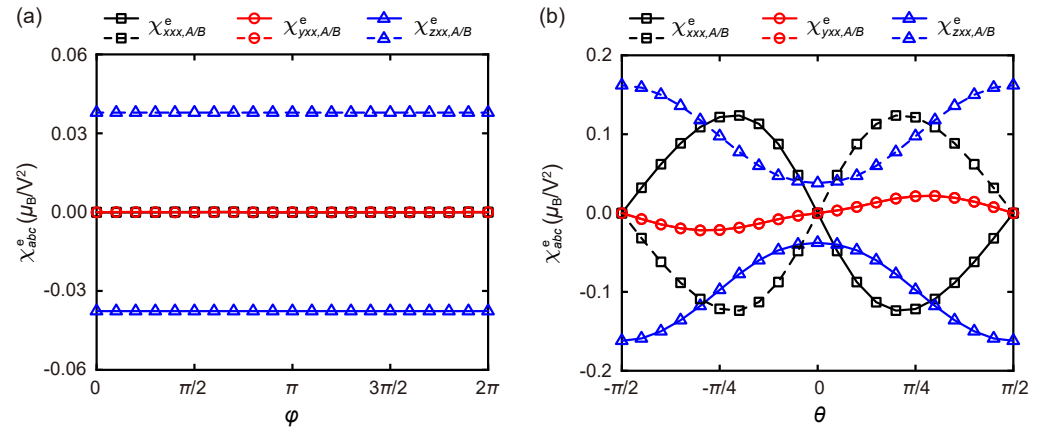

Fig. 3. $\mathcal{T}$-even nonlinear spin generations in an altermagnetic square lattice. (a) Evolutions of $\chi^{\rm e}_{xxx,i}$, $\chi^{\rm e}_{yxx,i}$, and $\chi^{\rm e}_{zxx,i}$ as functions of ϕ with fixed $\theta = 0$. (b) Evolutions of $\chi^{\rm e}_{xxx,i}$, $\chi^{\rm e}_{yxx,i}$, and $\chi^{\rm e}_{zxx,i}$ as functions of θ with $\phi = 0$. The chemical potential and the relaxation time are set to 1.0 eV and 0.05 ps, respectively.

opposite-spin sublattices. Besides, $\chi^{\rm o}_{zxx}$ reverses its sign at $\theta = 0$ for both the A and B sublattices, whereas $\chi^{\rm e}_{zxx}$ takes negative and positive values at various angles for the A and B sublattices, respectively. Correspondingly, $\chi^{\rm o}_{zxx}$ is odd with respect to $\theta = 0$, and $\chi^{\rm e}_{zxx}$ is even—indicating that they have opposite parities with respect to the magnetization direction.

In addition, we calculate nonlinear spin generations under the electric field along the y-axis. The results are similar to those obtained for an electric field along the x-axis, and they are provided in the SM.

4. First-Principles Calculations of Nonlinear Spin Generations. Based on the above symmetry analyses and model calculations, nonlinear spin generations can be expected in centrosymmetric altermagnets under electric current. Using first-principles based calculations, we study the nonlinear spin generations in a typical two-dimensional altermagnetic material, Fe_2Se_2O monolayer.[29] The details of the first-principles calculations are provided in the SM.

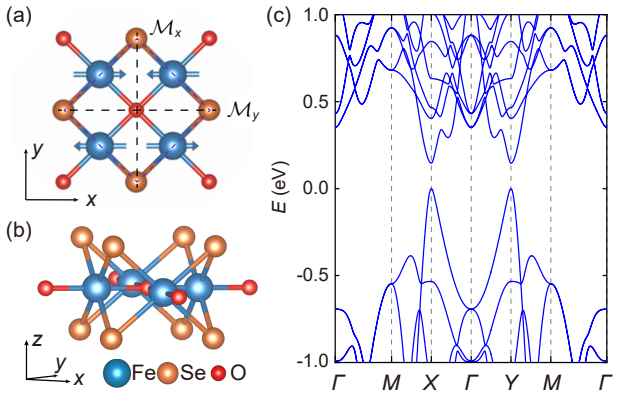

Fig. 4. Crystal and band structures of the Fe_2Se_2O monolayer. (a) Top view and (b) side view of the crystal structure. Blue, yellow, and red balls stand for Fe, Se, and O atoms, respectively. A unit cell of the monolayer is bounded by purple dashed lines. The arrows represent opposite spin directions on two inequivalent Fe atoms in a unit cell. (c) Band structure of the monolayer, with considering the SOC and the magnetization along the z-axis. The valence band maximum is set to zero energy.

Figures 4(a) and 4(b) demonstrate top and side views of the crystal structure of the Fe_2Se_2O monolayer, respectively. The monolayer has a tetragonal structure comprising three atomic layers. While the middle layer contains Fe and O atoms, the upper and lower layers consist solely of Se atoms and are arranged symmetrically with respect to the middle layer. A unit cell of the monolayer contains one chemical formula unit, i.e., two Fe atoms, two Se atoms, and one O atom. Each Fe atom is coordinated by two O and four Se atoms. These neighboring atoms form a distorted octahedron, with the calculated Fe–O and Fe–Se bond lengths being 2.02 Å and 2.64 Å, respectively.

The O–Fe–O bonds thus serve as the short axis of the distorted octahedron. It is seen that the directions of the short axes of the distorted octahedra surrounding the two Fe atoms in a unit cell are perpendicular to each other, a feature expected to induce perpendicular orbital ordering at the two Fe sites, analogous to the square model in Fig. 1. Besides, these two Fe atoms are related by mirror symmetries $\mathcal{M}_{x/y}$, located on Se–O–Se planes. Magnetic property calculations reveal that they carry opposite magnetic moments of magnitude $\sim 3.83\mu_B$. Therefore, the magnetic Fe atoms form an altermagnetic order.

Figure 4(c) shows the first-principles band structure of the Fe_2Se_2O monolayer, with considering the SOC and the magnetization aligned along the z-axis. In the band structure, two degenerate valleys appear at the X and Y points in both the valence and conduction bands, similar to our tight-binding results. The direct band gaps at the X and Y valleys are computed to be 146.2 meV. The band structure is consistent with previous calculations.[29]

Nonlinear spin generations are then calculated by Wannier-based tight-binding models with first-principles inputs. In the following, we take $\mathcal{T}$-odd out-of-plane spin generations under an electric field along the x-axis, i.e., $\chi^o_{zxx,A}$ and $\chi^o_{zxx,B}$, as examples, where the A and B sublattices correspond to two inequivalent Fe atoms with

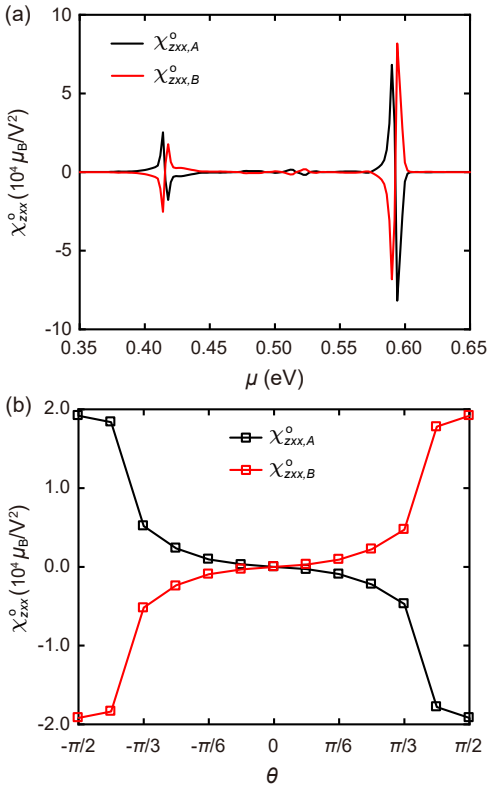

Fig. 5. Nonlinear spin generations in the Fe_2Se_2O monolayer. (a) Evolutions of $\chi^o_{zxx,A}$ and $\chi^o_{zxx,B}$ as functions of the chemical potential μ, with fixed $\theta = \pi/2$ and $\phi = 0$. (b) Evolutions of $\chi^o_{zxx,A}$ and $\chi^o_{zxx,B}$ as functions of θ, with fixed $\phi = 0$ and μ =0.42 eV. The conduction band minimum is set to zero energy.

opposite magnetic moments. As mentioned above, the out-of-plane spin generations are closely related to perpendicular magnetization switching in high-density storage devices. Figure 5(a) presents $\chi^o_{zxx,A}$ and $\chi^o_{zxx,B}$ as functions of the chemical potential μ. It is seen that $\chi^o_{zxx,A}$ and $\chi^o_{zxx,B}$ have equal magnitudes but opposite signs, indicating staggered nonlinear spin generations and agreement with the model calculations. The magnitudes of $\chi^o_{zxx,A}$ and $\chi^o_{zxx,B}$ vary with μ. When μ is approximately 0.4 eV above the conduction band minimum, $\chi^o_{zxx,A}$ and $\chi^o_{zxx,B}$ exhibit two neighboring peaks of opposite sign, with magnitudes of $1.3\times10^4\,\mu_B/V^2$ and $0.9\times10^4\,\mu_B/V^2$, respectively. These values exceed those of the nonlinear spin generations in the ferromagnetic $MnBi_2Te_4$ monolayer.[10] Therefore, considerable spin generations are expected in the Fe_2Se_2O monolayer by electron doping. Besides, further away from the conduction band minimum, higher peaks are found around 0.6 eV, with magnitudes of $3.4\times10^4\,\mu_B/V^2$ and $4.1\times10^4\,\mu_B/V^2$.

To elucidate the origin of considerable nonlinear spin generations in the Fe_2Se_2O monolayer, the momentum-resolved contributions to $\chi^o_{zxx,A}$ are provided in the SM. In the neighborhoods of crystal wave vectors with sizable contributions to $\chi^o_{zxx,A}$ and the chemical potentials corresponding to the peaks of $\chi^o_{zxx,A}$, several small-gap regions are found. According to the expressions for nonlinear spin generations in the SM, such generations are inversely pro-

portional to high powers of band energy differences. They thus strongly depend on the magnitudes of the band gaps. These small-gap regions dominantly contribute to the nonlinear spin generations in the Fe_2Se_2O monolayer, similar to the nonlinear Hall conductivities in, e.g., MnS,[30] and to the nonlinear spin generations in, e.g., $MnBi_2Te_4$.[10]

Figure 5(b) demonstrates $\chi^{\circ}_{zxx,A}$ and $\chi^{\circ}_{zxx,B}$ as functions of the canting angle θ, with fixed $\phi = 0$. The out-of-plane spin generations are staggered on the two Fe atoms. Moreover, their variations with θ are odd with respect to $\theta = 0$. These first-principles-based results fully support the model calculations in Fig. 2(b).

5. Discussion and Summary. It is noted that the Fe_2Se_2O monolayer studied above is merely a representative example of altermagnets hosting nonlinear spin responses to an electric field. A number of altermagnets have recently been designed,[31–33] and they are also expected to exhibit nonlinear spin generations. Through first-principles calculations, staggered and out-of-plane nonlinear spin generations are identified in other altermagnetic monolayers, V_2Se_2O[28] and Mn_2PSe,[33] as presented in the SM. These findings demonstrate that staggered and out-of-plane nonlinear spin generations are applicable to more altermagnets.

Through symmetry analyses and numerical calculations presented above, nonlinear spin generations in centrosymmetric altermagnets include staggered and uniform contributions between opposite-spin sublattices, different from those in centrosymmetric ferromagnets with only uniform contributions on magnetic atoms. The coexistence of staggered and uniform contributions, as shown in Figs. 2(c) and 2(d), indicates that the nonlinear spin generations are unequal in magnitudes between opposite-spin sublattices. Either the staggered spin generation itself or unequal spin generation can be used to regulate magnetic dynamics of opposite-spin sublattices.[23,24,34] Moreover, out-of-plane nonlinear spin components can be generated in centrosymmetric altermagnets and are expected to efficiently induce perpendicular magnetization switching without the need for an applied magnetic field, thereby contributing to the development of low-power spintronic devices. Besides, $\mathcal{T}$-odd and $\mathcal{T}$-even nonlinear spin generations have different parities with respect to the magnetization direction, as illustrated in Figs. 2 and 3. The joint effects of the $\mathcal{T}$-odd and $\mathcal{T}$-even parts are likely to induce complex magnetization dynamics. On the one hand, the sign-alternating $\mathcal{T}$-odd spin generations may hinder complete magnetization switching. On the other hand, they may reduce the critical switching current when cooperating with the sign-invariant $\mathcal{T}$-even nonlinear spin generations.[35] In addition, sign-alternating spin generations can be utilized in spin–orbit torque oscillators.

While the evolutions of the nonlinear spin generations with magnetization rotation are investigated in our tight-binding model and material candidates, the effects of in-plane electric field directions are discussed below. First, developing an approach to reverse the nonlinear spin generation via electric field control is crucial for deterministic magnetization switching. According to Eq. (1), the nonlinear spin generations remain unchanged upon reversal of the electric field, which is different from the linear counterpart. Considering the rotation of the electric field, we find that the out-of-plane $\mathcal{T}$-even spin generations satisfy $\delta s^{\rm e}_{z,A} = -\delta s^{\rm e}_{z,B} = \chi^{\rm e}_{zxx,A} E^2 \cos 2\gamma$ for the magnetization along the z-axis. Here, γ is the angle between the electric field and the x-axis. According to the relation, a $\pi/2$ rotation of the in-plane electric field reverses the sign of the nonlinear spin generation. As a result, electric fields along the x-axis and y-axis induce opposite δs_z on both the A and B sublattices, as corroborated by comparing Fig. 3 in the main text with Fig. S1 in the SM. Moreover, the electric field direction can also be used to induce unequal spin generation. For example, the out-of-plane $\mathcal{T}$-odd nonlinear spin generations have only staggered contribution when the electric field is along the x-axis or y-axis. By rotating the electric field away from the x- and y-axes, both staggered and uniform contributions emerge. The derivation of the nonlinear spin generation evolutions under electric field rotation is provided in the SM.

In addition, interfacial effects are difficult to avoid in realistic devices. Accordingly, linear spin generations may also arise due to the inversion-symmetry breaking. Combining this interfacial contribution with the nonlinear spin generations studied here is likely to result in generic unequal spin generations between opposite-spin sublattices. These linear and nonlinear spin generations can jointly modulate the magnetization dynamics, which is worth further study. The coexistence of staggered and uniform spin generations is also expected to extend to fully compensated ferrimagnetism.[36] The fully compensated magnetization in ferrimagnets is filling-enforced, whereas that in altermagnets is symmetry-enforced. Owing to the absence of symmetries connecting opposite-spin sublattices, the spin generations are expected to differ between these sublattices, and they are probably used to switch the Néel vector of ferrimagnets.

To conclude, we investigate nonlinear spin generations in centrosymmetric altermagnets. Staggered and out-of-plane spin generations are discovered in both a square altermagnetic model and typical altermagnets, e.g., Fe_2Se_2O monolayer. These nonlinear spin generations pave the way for electrically manipulating magnetic dynamics in compensated magnets with opposite-spin sublattices and for realizing perpendicular magnetization switching in high-density storage devices.

Acknowledgements. This work was supported by the National Natural Science Foundation of China (Grant Nos. 12374044, 11904173, and 12004186).

References

[1] Manchon A, Železný J, Miron I M, Jungwirth T, Sinova J, Thiaville A, Garello K, and Gambardella P 2019 *Rev. Mod. Phys.* **91** 035004

[2] Chappert C, Fert A, and Van D F N 2007 *Nat. Mater.* **6** 813

[3] Brataas A, Kent A D, and Ohno H 2012 *Nat. Mater.* **11** 372

[4] Železný J, Gao H, Výborný K, Zemen J, Mašek J, Manchon A, Wunderlich J, Sinova J, and Jungwirth T 2014 *Phys. Rev. Lett.* **113** 157201

[5] Železný J, Gao H, Manchon A, Freimuth F, Mokrousov Y, Zemen J, Mašek J, Sinova J, and Jungwirth T 2017 *Phys. Rev. B* **95** 014403

[6] Wadley P, Howells B, Železný J, Andrews C, Hills V, Campion R P,Novák V, Olejník K, Maccherozzi F, Dhesi S S, Martin S Y, Wagner T, Wunderlich J, Freimuth F, Mokrousov Y, Kuneš J, Chauhan J S, Grzybowski M J, Rushforth A W, Edmonds K W, Gallagher B L, and Jungwirth T 2016 *Science* **351** 587

[7] Bodnar S Y, Smejkal L, Turek I, Jungwirth T, Gomonay O, Sinova J, Sapozhnik A A, Elmers H J, Klaui M, and Jourdan M 2018 *Nat. Commun.* **9** 348

[8] Zhou X F, Zhang J, Li F, Chen X Z, Shi G Y, Tan Y Z, Gu Y D, Saleem M S, Wu H Q, Pan F, and Song C 2018 *Phys. Rev. Appl.* **9** 054028

[9] Selzer S, Salemi L, Deák A, Simon E, Szunyogh L, Oppeneer P M, and Nowak U 2022 *Phys. Rev. B* **105** 174416

[10] Xiao C, Liu H Y, Wu W K, Wang H, Niu Q, and Yang S A 2022 *Phys. Rev. Lett.* **129** 086602

[11] Xiao C, Wu W K, Wang H, Huang Y X, Feng X L, Liu H Y, Guo G Y, Niu Q, and Yang S A 2023 *Phys. Rev. Lett.* **130** 166302

[12] Hayami S, Yanagi Y, and Kusunose H 2019 *J. Phys. Soc. Jpn* **88** 123702

[13] Yuan L D, Wang Z, Luo J W, Rashba E I, and Zunger A 2020 *Phys. Rev. B* **102** 014422

[14] Hayami S, Yanagi Y, and Kusunose H 2020 *Phys. Rev. B* **102** 144441

[15] Liu P F, Li J Y, Han J Z, Wan X G, and Liu Q H 2022 *Phys. Rev. X* **12** 021016

[16] Šmejkal L, Sinova J, and Jungwirth T 2022 *Phys. Rev. X* **12** 031042

[17] Šmejkal L, Sinova J, and Jungwirth T 2022 *Phys. Rev. X* **12** 040501

[18] Han L, Fu X Z, Peng R, Cheng X K, Dai J K, Liu L Y, Li Y D, Zhang Y C, Zhu W X, Bai H, Zhou Y J, Liang S X, Chen C, Wang Q, Chen X Z, Yang L Y, Zhang Y, Song C, Liu J W, and Pan F 2024 *Sci. Adv.* **10** eadn0479

[19] Urata T, Hattori W, and Ikuta H 2024 *Phys. Rev. Mater.* **8** 084412

[20] Brekke B, Brataas A, and Sudbø A 2023 2023 *Phys. Rev. B* **108** 224421

[21] Orozco-Galvan G S, García-Fuente A, and Barraza-Lopez S 2024 *Phys. Rev. B* **109** 035141

[22] Attias L, Levchenko A, and Khodas M 2024 *Phys. Rev. B* **110** 094425

[23] Shao D F, Jiang Y Y, Ding J, Zhang S H, Wang Z A, Xiao R C, Gurung G, Lu W J, Sun Y P, and Tsymbal E Y 2023 *Phys. Rev. Lett.* **130** 216702

[24] Zhang P X, Chou C T, Yun H H, McGoldrick B C, Hou J T, Mkhoyan K A, and Liu L Q 2022 *Phys. Rev. Lett.* **129** 017203

[25] Hu S, Shao D F, Yang H L, Pan C, Fu Z X, Tang M, Yang Y M, Fan W J, Zhou S M, Tsymbal E, and Qiu X P 2022 *Nat. Commun.* **13** 4447

[26] You Y F, Bai H, Feng X Y, Fan X L, Han L, Zhou X F, Zhou Y J, Zhang R Q, Chen T J, Pan F, and Song C 2021 *Nat. Commun.* **12** 6524

[27] Engel H A, Rashba E I, and Halperin B I 2007 *Phys. Rev. Lett.* **98** 036602

[28] Ma H Y, Hu M L, Li N N, Liu J P, Yao W, Jia J F, and Liu J W 2021 *Nat. Commun.* **12** 2846

[29] Wu Y Z, Deng L, Yin X, Tong J W, Tian F B, and Zhang X M 2024 *Nano Lett.* **24** 10534

[30] Wang J Z, Zeng H, DuanWH, and Huang H Q 2023 *Phys. Rev. Lett.* **131** 056401

[31] Che Y X, Lv H F, Wu X J, and Yang J L 2025 *Phys. Rev. Lett.* **135** 036701

[32] Wang D H, Wang H Q, Liu L L, Zhang J T, and Zhang H J 2025 *Nano Lett.* **25** 498

[33] Liu C, Li X Y, Li X X, and Yang J L 2025 *Nano Lett.* **25** 9197

[34] Zhang S S, Wang Z A, Li B, Lu W J, Tian M L, Sun Y P, Du H F, and Shao D F 2025 arXiv: 2506.10786 [cond-mat.mtrl-sci]

[35] Ghosh S, Manchon A, and Železný J 2022 *Phys. Rev. Lett.* **128** 097702

[36] Liu Y C, Guo S D, Li Y P, and Liu C C 2025 *Phys. Rev. Lett.* **134** 116703